Doping-Spike PtSi Schottky Infrared Detectors with Extended Cutoff Wavelengths

T. L. Lin, J. S. Park, S. D. Gunapala, E. W. Jones, and H. M. Del Castillo

Center for Space Microelectronics Technology

Jet Propulsion Laboratory, California Institute of Technology

Pasadena, CA 91109

I. INTRODUCTION

Silicide Schottky infrared (IR) detectors offer promise of a low-cost, rugged, medium wavelength infrared (MWIR) thermal imaging technology with advantages in silicon-based fabrication, producibility, array size, response uniformity, and low I/f noise (1]. State-of-the-art 640 x 480- and 1024 x 1024-element PtSi focal plane arrays, with cutoff wavelengths ranging from 5.1 to 5.9 pm, are used for imaging in the 3-5 μm medium wavelength infrared (MWIR) region[2-5].

The spectral response of the silicide Schottky IR detector follows the modified Fowler equation, given by

$$\eta = C_1 \frac{(h\nu - \Psi_o)^2}{h\nu} \approx 1.24\, C_1 \lambda \left(\frac{1}{\lambda} - \frac{1}{\lambda_c}\right)^2 \qquad (1)$$

where η is the quantum efficiency (QE), C_1 is the emission coefficient, hv and λ are the energy and the wavelength of the incident photon, respective y, 'P_o is the optical potential barrier, and λ_c is the cutoff wavelength, given by

$$\lambda_c = \frac{1.24}{\Psi_o} . \qquad (2)$$

There is a great interest in extending the PtSi cutoff wavelength for long wavelength infrared (LWIR) operation in the 8-14 μm regime and for improved MWIR performance as given by Eq. 1. Previously, we have demonstrated extended PtSi cutoff wavelengths ranging from 5.7 to 22 μm by incorporating a thin p^+ layer (doping spike) at the PtSi/silicon interface[6,7]. The structure of the doping-spike Pt Si Schottk y infrared detectors is shown schematically in Fig. 1. The effective Schottky barrier height is determined by the combined effects of the image-force effect and the electric field due to the ionized dopants in the depletion region, as shown in Fig. 2. Therefore by incorporating a thin p^+ layer to take advantage of the

strong Schottky image force within ~2 nm from the PtSi/Si interface, as shown for two doping levels in Fig. 2 (a) and (b), the effective Schottky barrier can be reduced . The barrier reduction $\Delta\Psi$ due to the p^+ doping spike is given approximately by

$$\Delta\Psi \simeq \frac{q}{2\varepsilon_{Si}} N d^2 \qquad (3)$$

where N and d are the doping concentration and the thickness of the doping spike, respectively. Previous cutoff extension approaches utilized doping spikes thicker than 5 nm, resulting in the formation of potential spikes near the silicide/Si inter face, and thus required an additional tunneling process for the collection of photo-excited carriers which drastically reduced the detector response [8,9].

In this paper, we demonstrate the extended PtSi cutoff wavelengths and determine the maximum doping spike thickness, d_c, for the potential reduction without the tunneling effect. Thermionic-emission-limited dark current characteristics were observed for PtSi detectors with doping spikes thinner than d_c. For detectors with doping spike thicker than d_c, undesirable thermally -assisted-tunneling dark current characteristics were observed, and consequently lower operating temperatures were required to reduce the dark current.

IL CRITICAL SPIKE THICKNESS

The potential and the electric field in the Si near the silicide/Si for the doping-spike detector are given by [10]

$$\phi(x) = \left(\frac{q N (2d - x)}{2\varepsilon_{Si}} + E_d\right) x + \frac{q}{16\pi\varepsilon_{Si} x} \qquad \text{for } x < d \quad (5a)$$

$$= \sqrt{\frac{2 q N_s V}{\varepsilon_{Si}}}(x - d) - \frac{q N_s (x-d)^2}{2\varepsilon_{Si}} + \frac{q}{16\pi\varepsilon_{Si} x} + \left(\frac{q N d^2}{2\varepsilon_{Si}} + E d\right) \text{ for } x > d \quad (5.b)$$

$$E(x) = -\frac{d\phi}{dx} = \frac{q}{16\pi\varepsilon_{Si} x^2} - \frac{q N (d - x)}{\varepsilon_{Si}} - E_d \qquad \text{for } x < d \quad (6a)$$

$$= \frac{q}{16\pi\varepsilon_{Si}x^2} + \frac{qN_s(x-d)}{\varepsilon_{Si}} - E_d \qquad \text{for } x > d \quad (6.b)$$

where N_s is the doping concentration of the substrate, V is the bias voltage, E_d is the electric field at x = d due to the depleted region, given by $E_d = \sqrt{2qN_s(V+\phi)/\varepsilon_{Si}}$, and ϕ is the Schottky barrier height. As indicated in Eq. 6, E (x) is larger than zero for x near the silicide/Si interface and for x > d due to the strong Schottky effect. However, due to the degenerate doping concentration of the doping spikes, for spikes thicker than a critical thickness d_c, E(x) may be less than zero in the region x < d, resulting in the formation of a local potential maximum at x < d, as shown in Fig. 2 (b). This potential maximum facilitates hole accumulation at x = d, and the subsequent tunneling of holes into the substrate (thermally-assisted tunneling).

The critical spike thickness, d_c is given by equating E(x) = O, i.e..,

$$\frac{q}{16\pi\varepsilon_{Si}x^2} - \frac{qN(d-x)}{\varepsilon_{Si}} - E_d = 0 \qquad \text{for } x < d. \qquad (7)$$

Therefore,

$$d_c = \frac{3/4}{\pi^{1/3}N^{1/3}} - \frac{\varepsilon_{Si}E_d}{qN} \simeq \frac{3/4}{\pi^{1/3}N^{1/3}} \qquad (8)$$

Consequently, the critical spike thickness is determined mainly by the doping concentration of the spike, and is not sensitive to the bias voltage, especially for higher doping concentration, Figure 3 shows the critical thickness for the doping spikes as a function of the spike doping concentration. As the doping concentration increased from 10'9 to 102' cm^{-3}, the critical spike thicknesses decreases from 2.4 to 0.5 nm. Also shown in Fig. 3 are two curves for potential reduction of 0.05 and 0.15 eV, respectively, given by Eq. 3. A critical spike thickness of 2.1 nrn and a doping concentration of 1.5 x10] ^{9} cm^{-3} are required for the 0.05 eV potential reduction, which corresponds to a cutoff wavelength of 6.5 μm for the PtSi detector. For a longer cutoff wavelength, a smaller thickness and a significantly higher doping concentration for the doping spike are required. For example, a 0.7-nm-thick spike with a doping concentration of

$4 \times 10^{20}\ cm^{-3}$ is required for a 14 μm cutoff wavelength (().15 eV potential reduction).

The critical thickness and the corresponding doping concentrate ion for a specific potential reduction can be estimated by combining Eq. 3 and Eq. 8:

$$d_c = 0.211 \frac{q}{\pi\, \varepsilon_{Si}\, \Delta\Psi} \qquad (9)$$

$$N = 44.9 \frac{\pi^2\, \varepsilon_{Si}^3\, \Delta\Psi^3}{q3} \qquad (10)$$

Figure 4 shows the critical thickness and the corresponding doping concentration as a function of the potential reduction and the extended cutoff wavelength for PtSi detectors assuming a Schottky barrier height of 0.24 eV. To extend the cutoff wavelength, the thickness of the doping spike must be reduced with an increased doping concentration to obtain a larger potential reduction.

111. DETECTOR FABRICATION

Five PtSi detectors were fabricated on double-side polished Si (100) wafers with a resistivity of 30 Ω-cm. These detectors incorporated p^+ spikes at the PtSi/Si interface with thicknesses ranging from 0.7 to 1.1 nm and boron doping, concentrations ranging from 5 x 10^{19} to 2 x $10^{20}\ cm^{-3}$, and the PtSi layers were 4-rim-thick. The p^+ doping spikes were grown by MBE. The details of the MBE growth of the p^+ doping spikes and the PtSi formation are given elsewhere [6,7]. The device structure incorporated n-type guard rings which define the periphery of the active device areas in order to suppress the edge leakage. Neither an anti-reflection coating nor an optical cavity was incorporated in these test devices. The corresponding spike thicknesses and doping concentrations of these detectors are also indicated in Fig. 3.

IV. DETECTOR CHARACTERISTICS AND DISCUSS1ON

Thermionic-emission limited current characteristics were observed for all detectors. The typical I-V characteristics and the spectral response of a typical 6.5-μm-cutoff doping-spike PtSi detector (Sample B) are shown in Fig. 5 (a) and (b), respectively. The active device area is 4 x

10-4 cm2, and the thickness and the doping concentration of the doping spike are 0.9 nm and 6 x 1019 cm-3, respectively. The spectral response was measured at 40Kandbiased at-0.5 Vwith back-side illumination using a lOOOK blackbody source. The photoresponse is relatively insensitive to the bias voltage. Compared to conventional PtSi detectors which cutoff at -5.5 μm, the detector provides a significantly-improved 3-5 μm MWIR response. The cutoff wavelength can be further extended by increasing the doping-spike concentration. Figure 6 shows the spectral response ofsample Ewitha 14 pm cutoff wavelength. Due to its Fowler dependence (Eq. 1), the response decreases with the increasing wavelength.

The thermal potential barrier Ψ_t and the Richardson constant A** were determined by plotting J_o/T^2 versus 1/kT (the activation energy plot), where Jo is the dark current density and T is the absolute temperature. Figure 7 shows the activation energy plots at -0.5V bias of two typical doping-spike PtSi detectors (sample B and E). The thermal potential barriers were determined at the same -0.5 V bias of the spectral response measurement. Thermal potential barriers Ψ_t of 0.193 and 0.051 eV and Richardson constants A** of 72. and 0.1 A $cm^{-2}K^{-2}$ were measured for sample B and E, respectively.

The cutoff wavelengths, λ_c, and the corresponding optical potential barriers, Ψ_o, for the detectors were determined by the modified Fowler plot. Optical potential barriers Ψ_o ranging from 0.088 to 0.216 eV, corresponding to cutoff wavelengths ranging from 14 to 5.74 μm were determined from the linear portions of the modified Fowler plots. The spike thickness, the doping concentration, the thermal potential barrier Ψ_t, the Richardson constant A**, and the optical potential barrier Y'. are shown in Table 1 for comparison.

We note that sample D & E are in the tunneling region because their doping spikes are thicker than the critical thicknesses given by Eq. 8, as shown in Fig. 3. From Table 1, the Ψ_t for these two samples are dramatically lower than their Ψ_o (Y_o - Ψ_t of 0.056 and 0.037 eV for samples D and E, respectively) and the A** are smaller than those of the other samples. The Ψ_t for these samples are reduced as a result of the thermally-assisted tunneling effect, as shown in

Fig. 2 (b). Because of the additional tunneling process required for the collection of holes, smaller A** were observed for these samples. Similarly, the collection of the photo-excited holes involving the tunneling process is very difficult due to their short lifetime. Consequently, no reduction of the optical potential barriers Y'. were observed from the photoresponse measurements . The lower Y'$_t$ is undesirable because a lower operating temperature is required to reduce the dark current.

The doping spikes of the sample A, B, and C are thinner than the critical thickness, as shown in Fig. 3. From Table 1, we note that for these samples, the thermal potential barriers Ψ_t are similar to the optical potential barriers Ψ_o, with discrepancies less than 0.004 eV, indicating the absence of the tunneling effect. Therefore, doping spikes thinner than the critical thickness are desirable for cutoff extension to maximize the detector operating temperature.

V. SUMMARY

A doping spike technique for the extension of silicide Schottky IR detector cutoff wavelength has been developed and extended cutoff wavelengths have been observed for the doping-spike PtSi Schottky infrared detectors. The critic-al thickness of the doping spike without the tunneling effect has been determined, Thermionic-emission-limited and thermally-assisted tunneling dark current characteristics were observed for detectors with spikes thinner and thicker than the critical thickness, respectively.

ACKNOWLEDGMENTS

The work described in this report was performed by the Center for Space Microelectronics Technology, Jet Propulsion Laboratory, California Institute of Technology and was jointly sponsored by the National Aeronautics and Space Administration/Office of Advanced Concepts and Technology, the Ballistic Missile Defense Organization/Innovative Science and Technology Office, and the Air Force Rome Laboratory.

REFERENCES

[1] F. D. Shepherd, "Silicide infrared staring sensors," Proc, SPIE, vol. 930, p. 1, 1988.

2] D. J. Sauer, F. V. Shallcross, F. L. Hsueh, G. M. Meray, P. A, Levine, H. R. Gilmartin, T. S, Villani, B. J. Esposito, and J. R. Tower, "640 x 480 MOS PtSi IR sensors," Proc. SPIE, Vol. 1540, *Infrared Technology XVII*, edited by B. F. Andresen, M. Scholl, and I. J. Spiro, pp. 285-296 (SPIE, Bellingham, 1991).

[3] J. L. Gates, W. G, Connelly, T. D. Franklin, R. E. Mills, F. W. Price, and T. Y. Wittwer, "488 x 640-element platinum silicide Schottky focal plane. array," Proc. SPIE, Vol. 1540, *infrared Technology XVII*, edited by B. F. Andresen, M. Scholl, and I. J. Spiro, pp. 297-302, (SPIE, Bellingham, 1991).

[4] D. L. Clark, J. R. Berry, G. L. Compagna, M. A, Cosgrove, G. G. Furman, J. R, Heydweiller, H. Honickman, R. A. Rehberg, P. H. Solie, and E. T. Nelson, "Design and performance of a 486 x 640 pixel platinum silicide IR imaging system," Proc. SPIE, Vol. 1540, *Infrared Technology XVII*, edited by B. F. Andresen, M. Scholl, and I. J. Spiro, pp. 303-311, (SPIE, Bellingham, 1991).

[5] M. Kimata, N. Yutani, and S. N. Tsubouchi, "High performance 1040x 1040 element PtSi Schottky-barrier image sensor," Proc. SPIE. Vol. 1762, *Infrared Technology XVIII*, edited by B. F. Andresen and F. D. Shepherd (SPIE, Bellingham, 1992)

[6] T. L. Lin, J. S. Park, T. George, E. W, Jones, R. W. Fathauer, and J. Maserjian, "Long-wavelength PtSi infrared detectors fabricated by incorporating a p^+ doping spike grown by molecular beam epitaxy," Appl. Phys. Lett., vol. 62, pp. 3318-3320, 1993.

[7] T. L. Lin, J. S. Park, S. D. Gunapala, E. W. Jones, H. M. Del Castillo, M. M. Weeks and P. W. Pellegrini, "7-μm-Cutoff PtSi Infrared Detector for High Sensitivity MWIR Applications," submitted to IEEE Electron Devices Letters,

[8] C. Y. Wei, W. Tantraporn, W. Katz, G. Smith, "Reduction in the effective barrier height in PtSi-p-Si Schottky diodes by using low-energy ion-implantation," Thin Solid Films, 93, pp. 407-412, 1982.

[9] P. Pellegrini, M. Week, and C. E. Ludington, Proc. SPIE, Vol. 311, *Mosaic focal Plane Methodologies II*, edited by W. S. Chan and J. T. Hall, pp. 24-29 (SPIE, Bellingham, 1981).

[10] S. M. Sze, *Physics of Semiconductor Devices* (Wiley, New York, 1981), Chap. 5.

FIGURE CAPTIONS

Figure 1. Schematic diagram of doping-spike PtSi/p-Si Schottky infrared detector.

Figure 2. Calculated energy band diagrams of two doping-spike PtSi detectors within 8 nm from the PtSi/Si interface: (a) with a 0.9-nm-thick spike, $[B] = 10^{20}\ cm^{-3}$ and (b) with a 0.9-nm-thick spike, [B] = 2.3 x 1020 cm^{-3}. The bias voltage is -0.5 V.

Figure 3. Critical thickness for the doping spike versus spike doping concentration. Also shown are two curves for 0.05 and 0.15 eV potential reduction given by Eq. 3. The p^+ spike thicknesses and doping concentrations of the doping-spike PtSi samples are indicated.

Figure 4. Critical thickness and doping concentration of the doping spike as a function of the potential reduction.

Figure 5. Dark current characteristics (a) and the spectral response (b) of sample B. The active detector area is $4 \times 10^{-4}\ cm^2$.

Figure 6. Spectral response of a typical 14 μm cutoff backside-illuminated doping-spike PtSi detector (sample E). Neither an optical cavity nor an anti-reflection coating was incorporated in this detector.

Figure 7. Activation energy plots of sample B and sample E. Y'ı and A** were determined from the slopes and the intercepts of the linear fit curve fits, respectively.

TABLE 1. The spike thickness d, the spike doping concentration [R], the thermal potential barrier Ψ_t, the Richardson constant A**, the optical potential barrier Ψ_o , and the cutoff wavelength λ_c for the doping-spike PtSi detectors.

Sample #	d (rim)	[B] (cm^{-3})	Ψ_t (eV)	A** ($Acm^{-2}K^{-2}$)	Ψ_o (eV)	λ_c (pm)	$\Psi_o - \Psi_t$ (eV)
A	0.7	6×10^{19}	0.218	46	0.217	5.74	-0.001
B	0.9	6×10^{19}	o.193	72	0.189	6.56	-0.004
c	1.1	6×10^{19}	0.173	37	0.170	7.3	-0.003
D	1.1	1×10^{20}	0.112	0.16	0.168	7.38	0.056
E	0.9	2.3×10^{20}	0.051	0.10	0.088	14.1	0.037

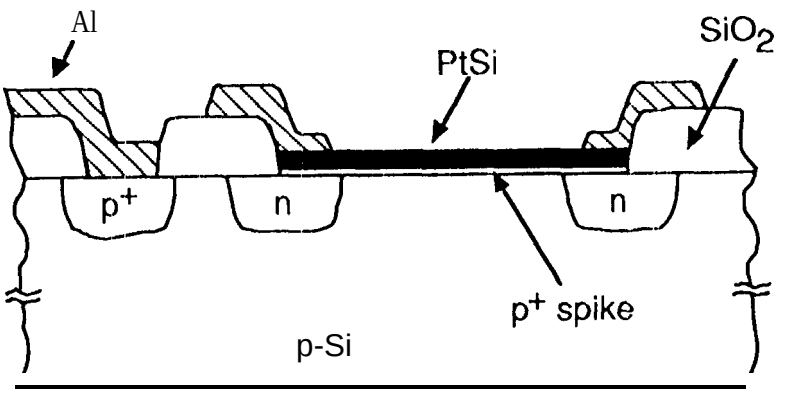

T. Lin
Figure 1

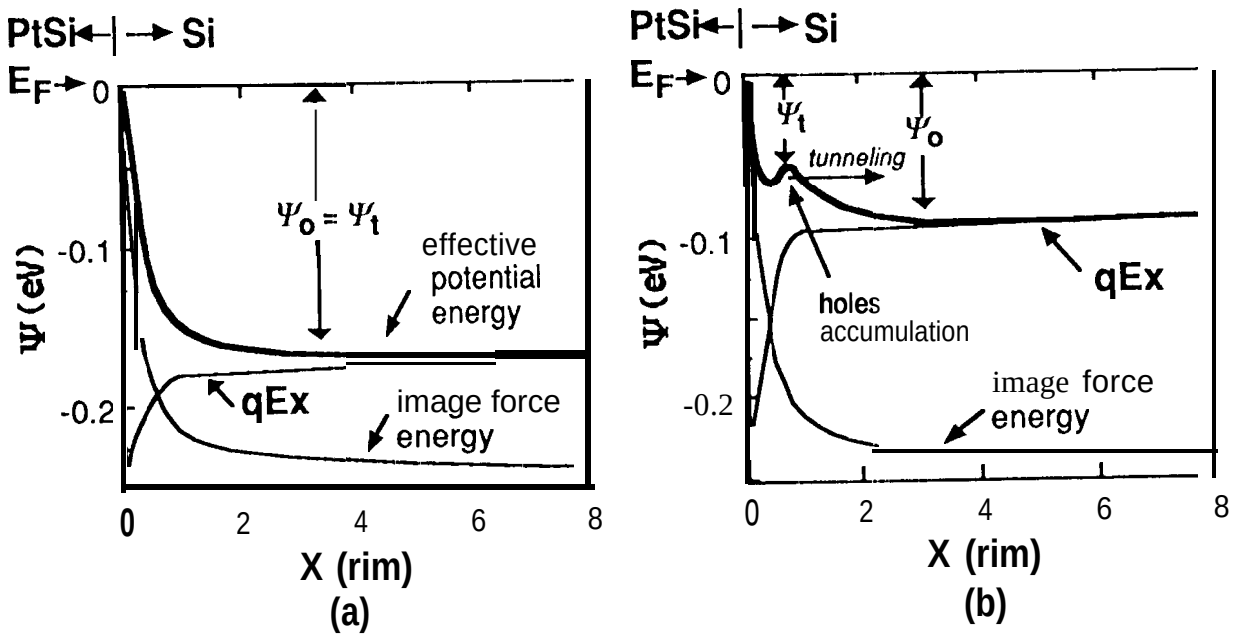

T. Lin
Figure 2

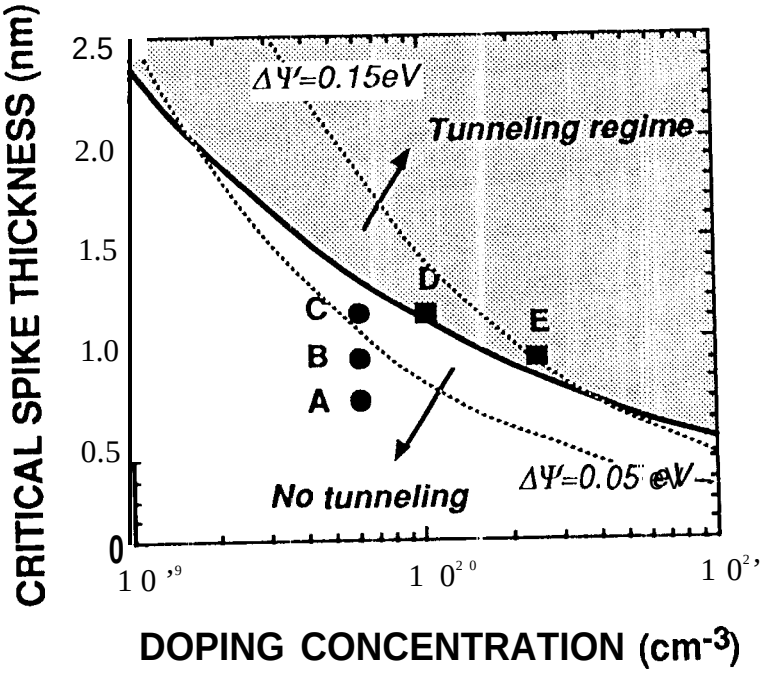

T. Lin
Figure 3

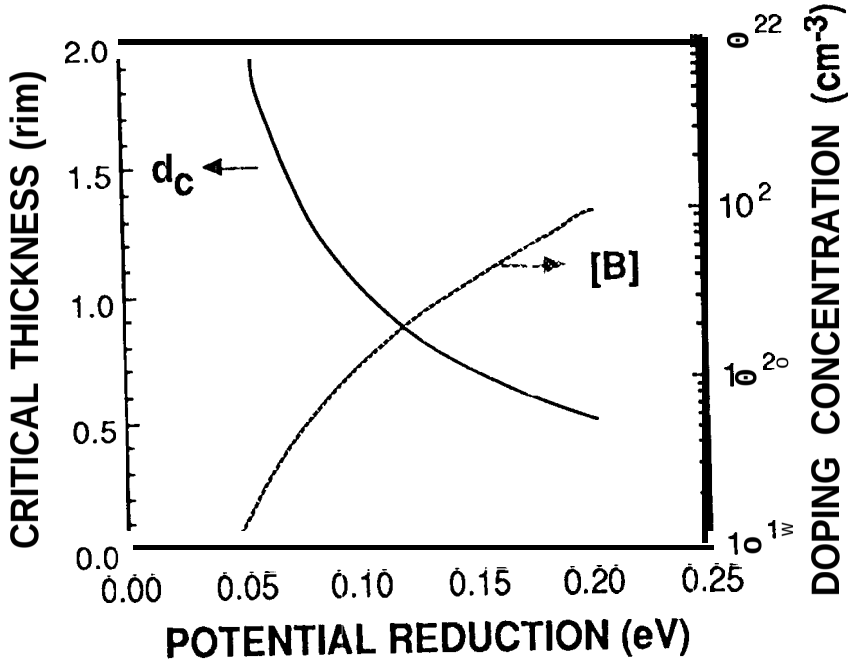

T. Lin
Figure 4

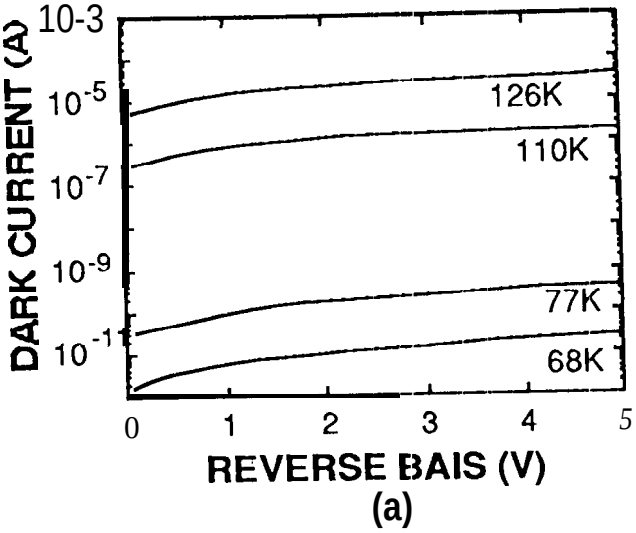

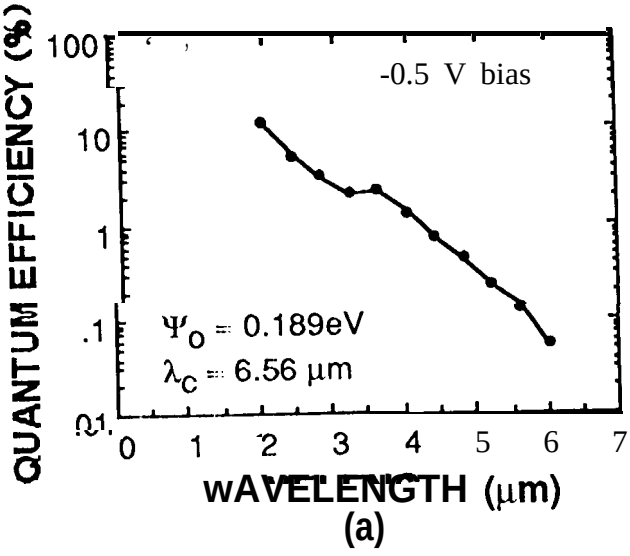

T. Lin
Figure 5

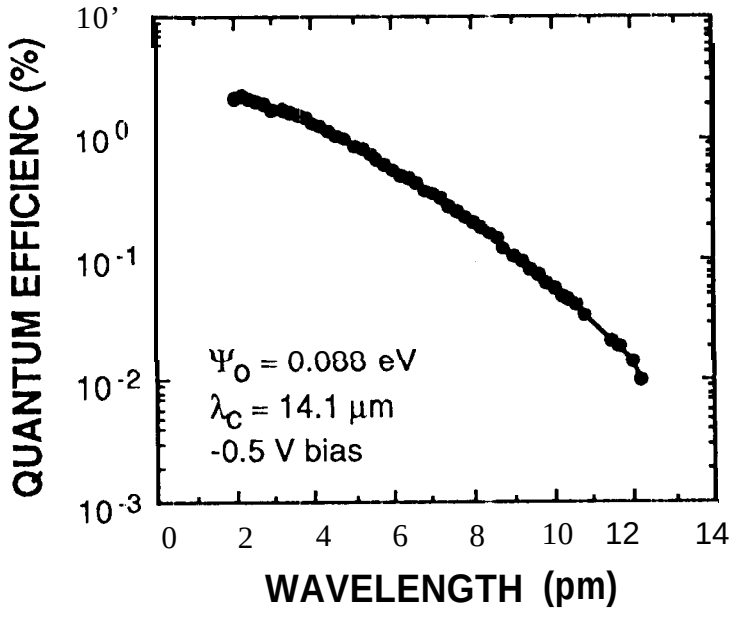

T. Lin
Figure 6

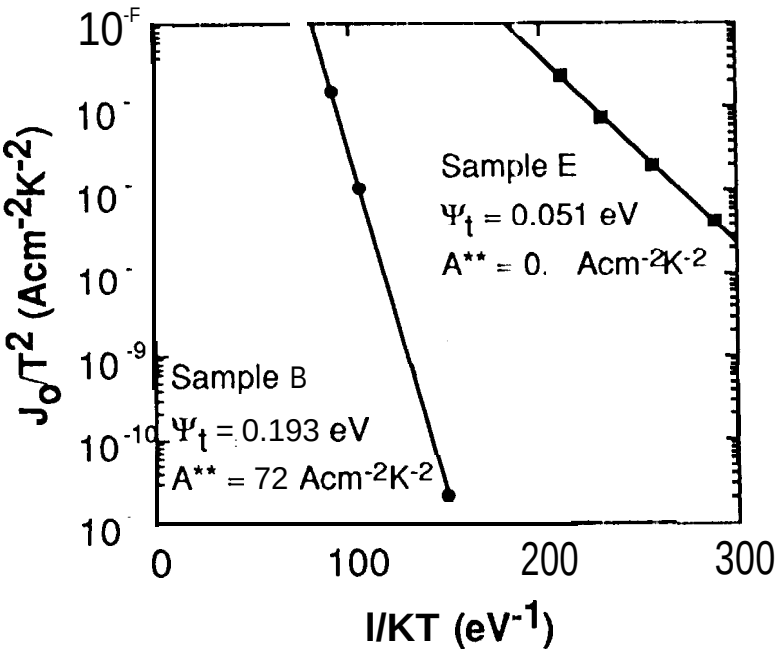

T. Lin
Figure 7